RSC Advances

ROYAL SOCIETY OF CHEMISTRY

www.rsc.org/advances

A strategy to enhance overall efficiency for dye-sensitized solar cells with a transparent electrode of nickel sulfide decorated with poly (3, 4-ethylenedioxythiophene)

Xingping Ma [a], Gentian Yue [a,*], Jihuai Wu [b], Zhang Lan [b], Jeng-Yu Lin [c,*]

[a] *Key Laboratory of Photovoltaic Materials of Henan and School of Physics & Electronics, Henan University, Kaifeng 475004, China*;

[b] *Institute of Material Physical Chemistry, Huaqiao University, Quanzhou 362021,China*;

[c] *Department of Chemical Engineering, Tatung University, Taipei 104, Taiwan*

Keywords: Nickel sulfide; poly (3, 4-ethylenedioxythiophene); counter electrode; transparent; dye-sensitized solar cells

Abstract: To improve power conversion efficiency of dye-sensitized solar cell (DSSC), a DSSC based on

a∗ Corresponding author. +86 371 23881602, E-mail address: yuegentian@henu.edu.cn (G. Yue);

c∗ Corresponding author. +886 225925252x2561 119, E-mail address: jylin@ttu.edu.tw (J.-Y. Lin).

transparent counter electrode (CE) and a piece of new alunimium foil as a reflector was devised. Owing to the sunlight irradiation simultaneously from the rear side, more dye molecules are excited and more carriers are generated, the short-circuit current density and power conversion efficiency enhancement greatly. In this work, a transparent electrode of nickel sulfide decorated with poly (3, 4-ethylenedioxythiophene) (NiS/PEDOT) was prepared by two-step electrochemical/chemical process. The NiS/PEDOT hybrid electrode takes the advances of NiS and PEDOT as counter electrode for DSSC. The incorporation of PEDOT conductive networks in fact provides additional pathways for electron transport in the NiS/PEDOT hybrid electrode, and thus facilitates increasing the charge-transfer rate at the interface of CE/electrolyte. The DSSC based on the NiS/PEDOT CE and a piece of new alunimium foil as a reflector achieved higher power conversion efficiency of 8.47% compared to the DSSC irradiated from the front only (7.77%) under the irradiation of 100 $mW \cdot cm^{-2}$ (AM 1.5G). This strategy of double irradiation are of practical maneuverability and reference use than that of used two lights or mirrors, which provides a new and promising approach for enhancing the photovoltaic performances of solar cells in practice.

1. Introduction

Dye-sensitized solar cell (DSSC) has received considerable attention due to its unique advantages, such as relative low-cost, high efficiency, facile fabrication, environmentally friendly, etc.[1,2] The highest power conversion efficiency of DSSC has achieved over 13%.[3] As an important component of DSSC, counter electrode (CE) plays an important role in the performance of DSSC. Platinum (Pt), the widely served as CE material, exhibits excellent catalytic activity but high cost, and the problem of Pt dissolution in corrosive electrolyte severely restricts the large-scale application for DSSCs.[4] Consequently, seeking Pt-like catalyst with inexpensive has become one of the priorities in the field. Among the various types of Pt-free CE alternative, carbon materials, organic conducting polymers and transition metal compounds[5-13] have been extensive attempts as CEs for DSSCs in recent years. Meanwhile, it is also found that the composite materials consisted of carbon materials, organic conducting polymers or transition metal compounds with great electrocatalytic ability in iodide/triiodide (I^-/I_3^-) electrolyte served as CEs in DSSCs.[14-18] Xiao et al. reported that the DSSC assembled with the PEDOT/MWCNT CE exhibited a superior photovoltaic conversion efficiency of 7.03% compared to that of the DSSC with Pt CE (5.88%).[19] Wang reported the use of two selenides, $Co_{0.85}Se$ and $Ni_{0.85}Se$, served as CE in DSSC and the high power conversion efficiencies (*PCEs*) of up to 9.40% were obtained.[20]

Based on the above analysis, it can be inferred that the electrocatalytic property of the composite catalytic materials made from organic conducting polymers and transition metal compounds as CEs for the DSSCs will be improved greatly. On the other hand, enhanced the sunlight harvest can improve the *PCE* of solar cells.[21,22] Consequently, a DSSC introduced a piece of new alunimium foil as a reflector to enhance the light capture based on the transparent NiS/PEDOT CE was envisaged. The transparent NiS/PEDOT CE with low charge transfer resistance as well as excellent electrocatalytic activity for I_3^- reduction was characterized by cyclic voltammetry (CV) and electrochemical impedance spectroscopy (EIS). The incident light perpendicularly irradiated on the front side of the DSSC, and the transmitted light through the DSSC and round the edges of the device was reused by reflecting it onto the rear side of the DSSC. The DSSC with NiS/PEDOT CE and a piece of new alunimium foil achieved an enhanced photovoltaic conversion efficiency of 8.47% under the irradiation of 100 $mW \cdot cm^{-2}$ (AM 1.5G).

2. Experimental

2.1 Preparation of NiS/PEDOT counter electrode

Firstly, the NiS CE was prepared by using the electrodeposition method as follows.[23,24] Briefly, the electrodeposition was carried out with an electrochemical analyzer system (CHI660E, Shanghai Chenhua Device Company, China). All experiments were implemented in a three-electrode cell, including one Pt foil as CE, one Ag/AgCl electrode as reference electrode, and fluorine-doped tin oxide transparent (FTO) with an exposed area of 0.64 cm^2 as working electrode. The base electrodeposition solution consisted of 0.05 M nickel (II) chloride hexahydrate ($NiCl_2 \cdot 6H_2O$, 98%) and 1.0 M thiourea (≥ 99.0%) solution in 50 ml deionized water and treated by ultrasonication for 30 min. A constant current density of 10 $mA \cdot cm^{-2}$ was served for electrodeposition. The obtained NiS CE was put into 4-aminothiophenol (4-ATP)/ethanol solution for 10 min, and vacuum oven at 100□ for 12 h.

Secondly, the modification of NiS CE was immersed in 0.015 M 3, 4-ethylenedioxythiophene (EDOT) monomer solution (signed A solution), and then 25.1 $g \cdot L^{-1}$ ammonium persulphate solution (signed B solution) and 0.18 mM ferric sulfate solution (signed C solution) were fast added into A solution at 4℃ for 6 h, resulting in an in-situ polymerization reaction of EDOT monomers into the NiS nanopaticles (the preparation route shown in Fig. 1).

For comparison, the PEDOT CE was prepared by immersing 0.015 M EDOT, 25.1 $g \cdot L^{-1}$ ammonium persulphate and 0.18 mM ferric sulfate solution at 4℃ for 6 h; the Pt CE was electropolymerization from the plating solution consisted of 0.01 M H_2PtCl_6 and 14 wt% HCl.

2.2 Fabrication of DSSC

The TiO_2 anode was prepared as described previously.[25,26] The dye was loaded by immersing the TiO_2 anode in the 0.3 mM of dye Z-907 ethanol solution for 12 h. Thus the dye-sensitized TiO_2 anode with thickness of 8-10 μm was obtained. The DSSC was fabricated by injecting the liquid electrolyte (0.05 M of I_2, 0.1 M of LiI, 0.6 M of tetrabutylammonium iodide and 0.5 M of 4-tert-butyl-pyridine in acetonitrile) into the aperture between the dye-sensitized TiO_2 electrode and the CE. The two electrodes were clipped together and wrapped with thermoplastic hot-melt Surlyn.

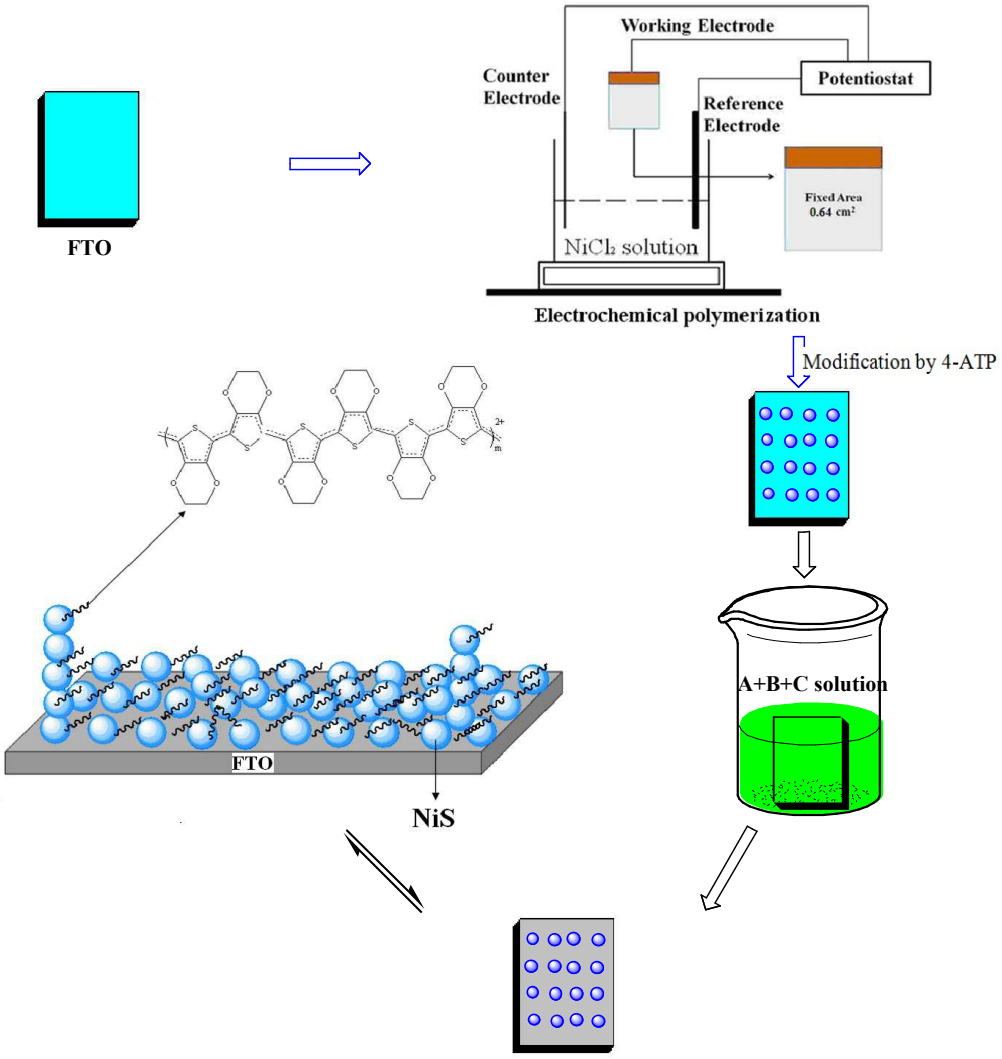

Fig. 1 NiS/PEDOT coated on FTO substrate by two-step electrochemical/chemical process.

2.3 Characterization

The surface morphology of the sample was observed by using JSM-7001F FE-SEM. CV and EIS were conducted by using a computer-controlled electrochemical analyzer (CHI 660E, CH Instrument). The electrolyte used in the DSSC test was also injected into the symmetric dummy cells for EIS measurements. EIS was carried out under the simulating open-circuit conditions at ambient atmosphere, sealing with thermoplastic hot-melt Surlyn and leaving an exposed area of 0.64 cm^2. The frequency of applied sinusoidal AC voltage signal was varied from 0.1 Hz to 10^5 Hz and the corresponding amplitude was kept at 5 mV in all cases.

The photovoltaic test of DSSC with an exposed area of 0.4×0.7 cm^2 was carried out by measuring

photocurrent-photovoltage (*J-V*) character curve under white light irradiation of 100 mW·cm^{-2} (AM 1.5 G) came from the solar simulator (XQ-500W, Shanghai Photoelectricity Device Company, China) in ambient atmosphere. One piece of new aluminum foil was put under the DSSC used as reflector to reflect the lights (the light irradiation of about 40 mW·cm^{-2}) from the rear direction of counter electrode. The fill factor (*FF*) and the power conversion efficiency (*PCE*) of DSSC were calculated according to the following equations:

$$PCE(\%) = \frac{V_{max} \times J_{max}}{P_{in}} \times 100\% = \frac{V_{oc} \times J_{sc} \times FF}{P_{in}} \times 100\% \quad (1)$$

$$FF = \frac{V_{max} \times J_{max}}{V_{oc} \times J_{sc}} \quad (2)$$

where J_{sc} is the short-circuit current density (mA·cm^{-2}); V_{oc} is the open-circuit voltage (V); P_{in} is the incident light power (mW·cm^{-2}), J_{max} (mA·cm^{-2}) and V_{max} (V) are the current density and voltage at the point of maximum power output in the *J–V* curve, respectively.

3. Results and discussion

3.1 Surface morphology and composition of the samples

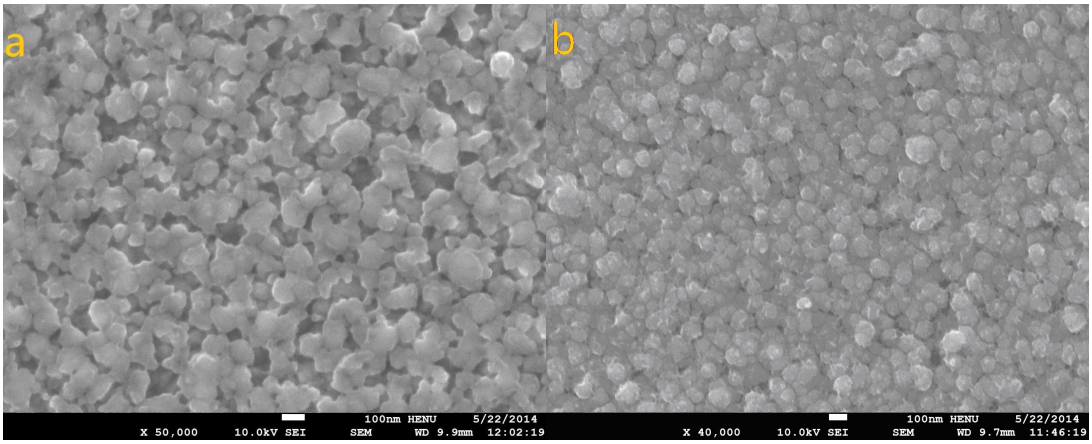

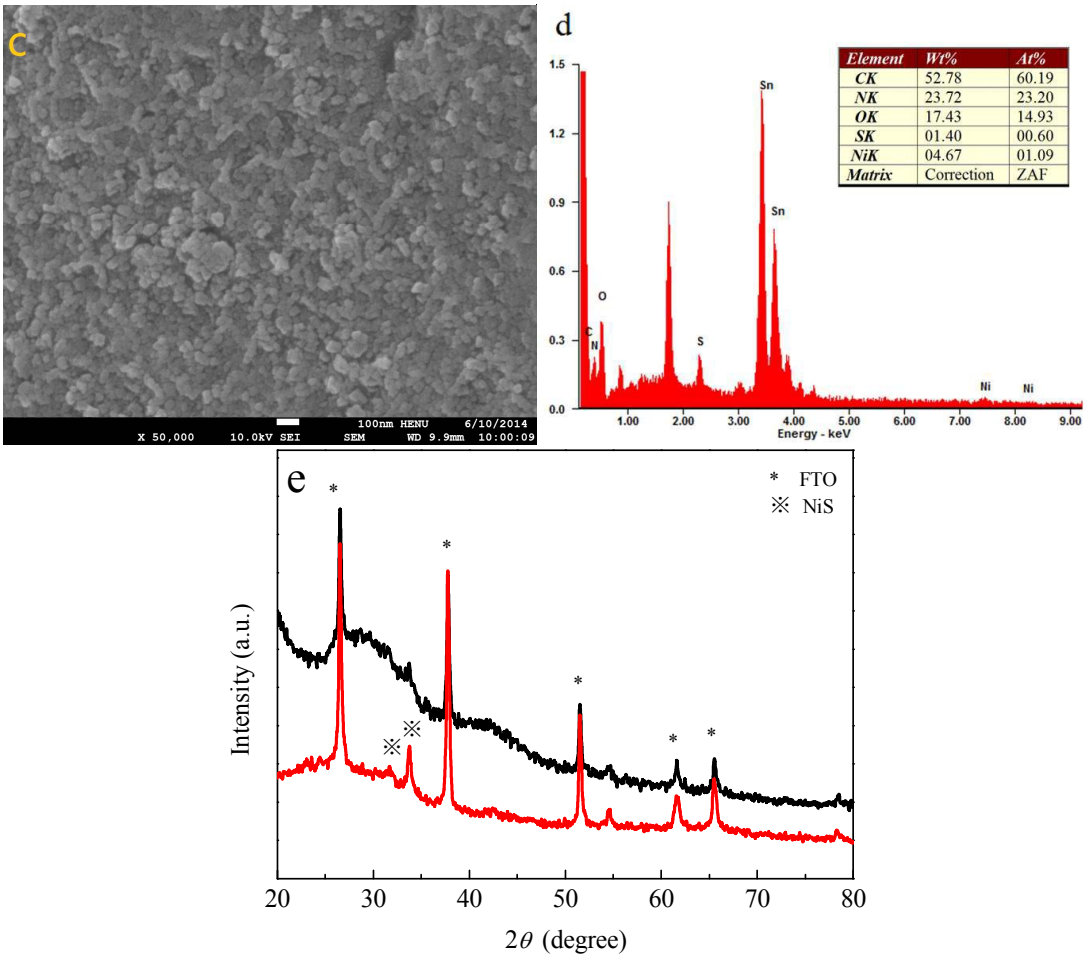

Fig. 2 SEM images of PEDOT (a), NiS (b) and NiS/PEDOT (c) films; the EDS image of NiS/PEDOT CE (d); XRD patterns of FTO and NiS (e).

Fig. 2 shows the SEM images of PEDOT, NiS, NiS/PEDOT films and the EDS image of NiS/PEDOT CE. Fig. 2a exhibits that the PEDOT film using the in-situ polymerization shows a network structure surface morphology on FTO substrate, which is favorable to the penetration of electrolyte. As seen as in Fig. 2b, it can be obtained that the NiS nanoparticles uniformly arranged on FTO substrate with perfect smooth surface. Compared to Fig. 2a and 2b, the NiS/PEDOT film (Fig. 2c) interestingly presents a smooth morphology of NiS nanoparticles and PEDOT net-work integrated tightly, intercross and penetrate. Such structure will provide additional pathways for electron transport in the NiS/PEDOT hybrid electrode, favors the permeation of iodide/triiodide electrolyte and the sunlight transmission, and thus accelerates photogenerated charge carriers' production and transportation.[27] The EDS analysis of the NiS/PEDOT hybrid electrode (Fig.2d) indicates the presence of C, N, O, S and Ni elements, which demonstrates qualitatively the preparation of NiS/PEDOT on FTO substrate. To further

characterize the sulfide composition, the XRD characterization was also carried out and presented in Fig.2e. For comparison, the XRD of FTO was also tested under the same conduction. From the XRD spectrum, it can be seen that the signals of FTO were very strong, which almost covered the signals of sulfide, but the crystalline phase of NiS still can be observed clearly at 33.8°, according to the Joint Committee on Powder Diffraction Standards (JCPDS card no. 3-1149). From the XRD data, it can be confirmed that the NiS film was obtained using electrochemical deposition method.

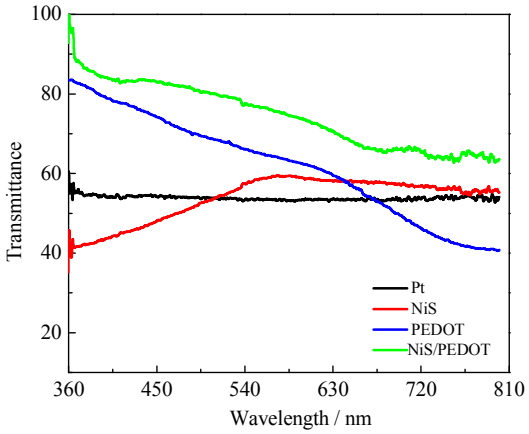

Fig. 3 UV-vis transmittance spectra of four CEs

Fig. 3 exhibits the transmittances of the four kinds of CEs with the best electrocatalytic activity. The Pt CE has average transmittance of about 52% in wavelength range 360-800 nm. The PEDOT CE shows the better transmittance in wavelength range 360-670 nm than Pt CE. This is due to high reflective of Pt CE. The NiS CE displays lower transmittance than PEDOT CE in wavelength range 360-640 nm with long deposition time to meet the need of catalytic active. The NiS/PEDOT electrode shows improved transmittance in wavelength range 360-800 nm than Pt, NiS, PEDOT CEs by modifying with 4-ATP. This is due to that 4-ATP as a bridging agent improves the combination of FTO or NiS layer via –SH. The NiS/PEDOT electrode shows higher transmittance in dye sensitized range 400-750 nm and therefore is a better candidate than Pt as CE for the DSSC.

3.2 Electrochemical properties

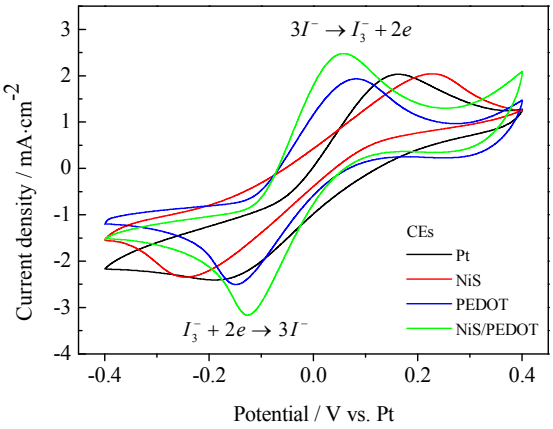

Fig. 4 Cyclic voltammograms for the Pt, NiS, PEDOT and NiS/PEDOT counter electrodes with the scan rate of 50 mV·s^{-1}.

To investigate the electrocatalytic ability of the various CEs, CV curves are obtained in the scan interval ranging from −0.4 to 0.4 V vs. Pt according to the previous reports.[28,29] The anodic peaks are responsible for the reaction of $3I^- \rightarrow I_3^- + 2e^-$, and the cathodic peaks are vital for the performance of DSSC and correspond to $I_3^- + 2e^- \rightarrow 3I^-$. The cathodic peak potential (V_{pc}) is inversely correlated and current density (I_{pc}) is positive correlated to the catalytic activity of CE.[30] Fig. 4 shows the CVs for the Pt, PEDOT, NiS and NiS/PEDOT CEs at the scan rate of 50 mV·s^{-1}. The corresponding parameters of I_{pc} and V_{pc} obtained from the CV curves are listed in Table 1. From Table 1 and Fig. 4, the Pt, PEDOT and NiS CEs have a similar $|I_{pc}|$. This signifies that both NiS and PEDOT CEs possess the Pt-like electrocatalytic activity for I_3^- reduction. The V_{pc} of the above mentioned CEs increases in the order of NiS (-0.25±0.01 V) < Pt (-0.18±0.01 V) < PEDOT (-0.14±0.01 V) < NiS/PEDOT (-0.12±0.01 V), which is immediately responsible for the lower overpotential loss in the NiS/PEDOT CE than that of the NiS and PEDOT CEs since the highly conductive PEDOT was incorporated within NiS nanopaticles. Consequently, the fact of I_{pc} and V_{pc} both indicate that the electrocatalytic activity and conductivity of NiS/PEDOT CE can be further enhanced for their synergistic catalytic effect of NiS and PEDOT originated from their excellent intrinsic electrocatalytic activity and electrical conductivity.

Also, the diffusion coefficient (Dn) of I_3^- for the Pt, NiS, PEDOT and NiS/PEDOT CEs can be estimated to be 2.78×10^{-6}, 2.63×10^{-6}, 3.00×10^{-6} and 4.79×10^{-6} cm^{-2}·s^{-1}, respectively, according to the Randles-Sevcik equation as following. [31]

$$I_{pc} = Kn^{1.5}AC(Dn)^{0.5}v^{0.5} \quad (3)$$

where I_{pc} is the cathodic current densities; K is the constant of 2.69×10^5; n means the number of electrodes contributing to the charge transfer (here n=2); A is the area of the CE; C and v represent the concentration of I_3^-

species and the scan rate, respectively.

Thus, it can be found that the diffusivity for the NiS/PEDOT CE is slightly larger than that of the Pt, PEDOT and NiS CEs, which displays that the NiS/PEDOT CE possesses a much faster rate for I^-/I_3^- reaction.

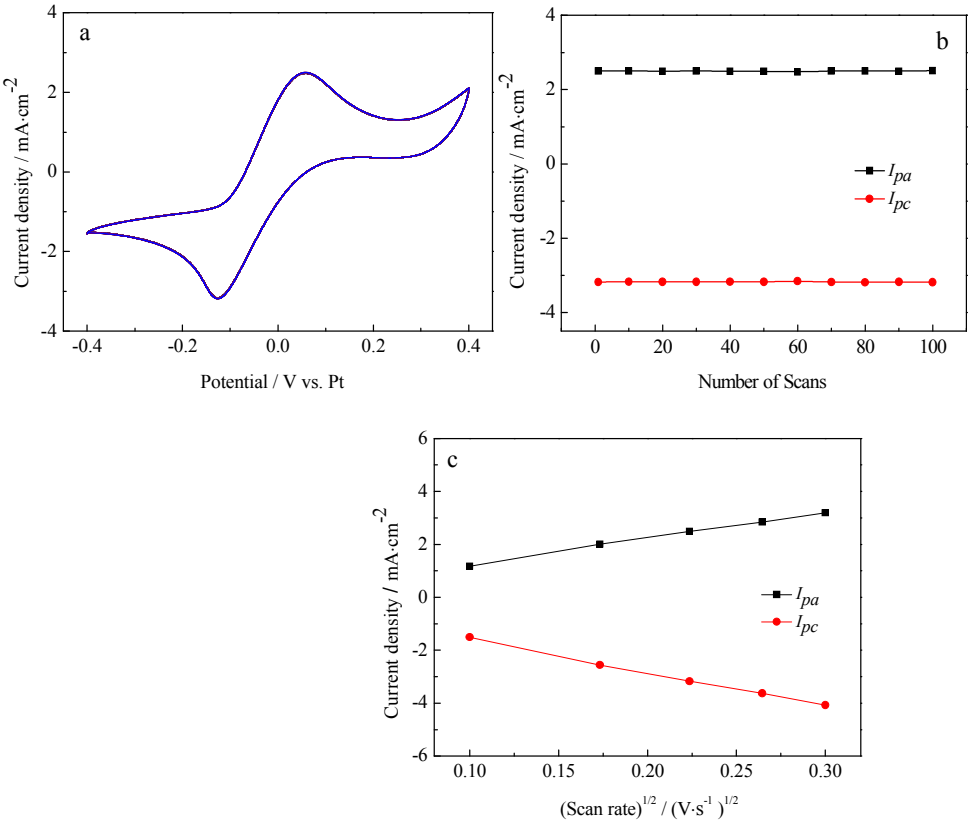

Fig. 5 The CVs for the NiS/PEDOT CE in I^-/I_3^- electrolyte (a); the behaviors of I_{pa} and I_{pc} in CVs for the sample (b); and the influences of the scan rate on the redox peaks current density (c).

Fig. 5a and Fig. 5b show the 100 successive CV cycles of the NiS/PEDOT CE and the behaviors of max anode peak current density (I_{pa}) and I_{pc} at a scan rate of 50 $mV \cdot s^{-1}$. Both the max I_{pa} and I_{pc} have not changed significantly with the cycle number increasing, indicating that the NiS/PEDOT CE possesses great electrochemical reversibility and stability.[32] Fig. 5c displays that the current density *versus* $(\text{scan rate})^{1/2}$ plots have a good linear relationship. This phenomenon can be apparently found that the adsorption of iodide species is almost no effect by redox reaction on the NiS/PEDOT CE surface, indicating no specific interaction between I^-/I_3^- redox couple and the NiS/PEDOT CE as like as Pt electrode.

Table 1 The electrochemical performance parameters made from EIS and CVs based on the various counter electrodes.

CEs	R_s ($\Omega \cdot cm^2$)	R_{ct} ($\Omega \cdot cm^2$)	Z_w ($\Omega \cdot cm^2$)	I_{pc} ($mA \cdot cm^{-2}$)	V_{pc} (V)	J_0 ($mA \cdot cm^{-2}$)
Pt	6.30±0.01	2.99±0.01	1.60±0.01	-2.41±0.01	-0.18±0.01	1.38±0.01
NiS	6.98±0.01	5.96±0.01	2.79±0.01	-2.34±0.01	-0.25±0.01	1.15±0.01
PEDOT	7.14±0.01	4.20±0.01	9.35±0.01	-2.50±0.01	-0.14±0.01	1.27±0.01
NiS/PEDOT	7.22±0.01	2.85±0.01	0.67±0.01	-3.16±0.01	-0.12±0.01	1.59±0.01

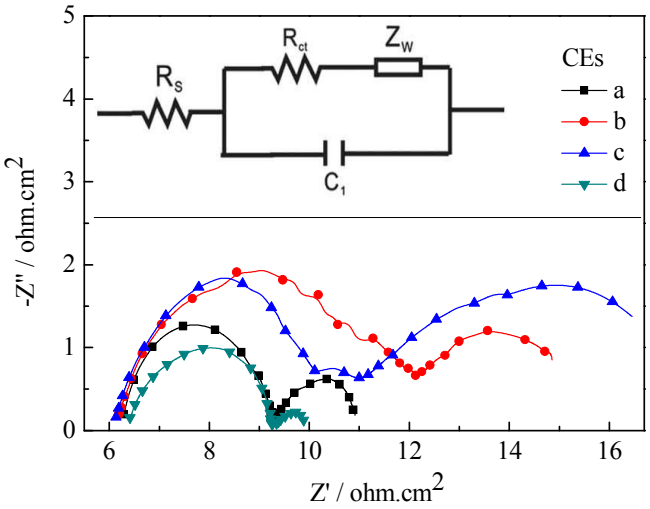

Fig. 6 EIS of the symmetrical Pt (a), NiS (b), PEDOT (c), and NiS/PEDOT (d) CEs for I^-/I_3^- redox couple and the equivalent circuits.

Fig. 6 represents the Nyquist plots of the Pt, NiS, PEDOT and NiS/PEDOT CEs. The equivalent circuit is shown in its inset, and the related electrocatalytic performance parameters are summarized in Table 1, in which the high-frequency intercept on the real axis represents the series resistance (R_s) including the sheet resistance of two identical CEs and the electrolytic resistance; the first semicircle at high frequency refers to the charge-transfer resistance (R_{ct}) for the I_3^- reduction at the CE|electrolyte interface, and the second semicircle at low frequency represents the Nernst diffusion impedance (Z_w) corresponding to the diffusion resistance of the I^-/I_3^- redox species, respectively.[33,34] As seen as in Fig. 6 and Table 1, the NiS, PEDOT and NiS/PEDOT CEs are provided with a similar R_s of about 6.9～7.2 $\Omega \cdot cm^2$, indicating the CEs are firmly bonded to the FTO substrate as well as Pt electrode, which has discussed at the anterior CV section. The R_{ct} is inversely correlation with the electrocatalytic activity of CE and the order of CEs follows NiS > PEDOT > Pt > NiS/PEDOT as shown as in Table 1. This indicates that the NiS/PEDOT CE possesses the comparable reaction rate of the I^-/I_3^- regeneration on their surface to that of the Pt CE. It is noticeable that the considerably lower R_{ct} value can be obtained for the NiS/PEDOT CE

while the conductive PEDOT was incorporated as the extra channels for electron transport and synergistic effect.[35] Furthermore, the Z_w arises from limitations in the mass transportation of the electrolyte can not be ignored, especially in the PEDOT film. Compared to the Pt and NiS CEs, the PEDOT CE has a larger Z_w of 9.35±0.01 Ω·cm^2, which is related to its film thickness. However, the Z_w of NiS/PEDOT CE is found of 0.67±0.01 Ω·cm^2, which is much smaller than that of Pt, NiS and PEDOT CEs. This result shows that the electrocatalytic performance of the NiS/PEDOT CE, upon incorporating with highly conductive PEDOT network, is dramatically improved.

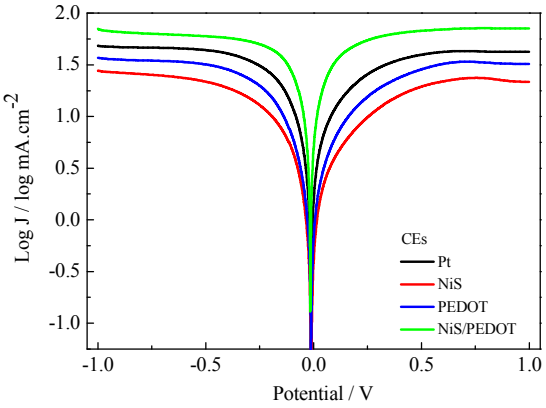

Fig. 7 Tafel curves of the various counter electrodes.

In additional to the EIS analyses, Tafel test is another mean to aid investigation the interfacial charge-transfer properties of the I^-/I_3^- redox couple on the CEs. Fig. 7 gives the Tafel curves of Pt, NiS, PEDOT and NiS/PEDOT CEs. The curves present the logarithmic current density as a function of the potential. The detailed polarization analyses can be referred to the previous studies.[36] The exchange current density (J_0) is obtained as the intercept of the extrapolated linear region of the curve when the over-potential is zero, which is inversely related to R_{ct} as illustrated in Eqn. (4),[37] and is therefore considered as a quantitative factor for evaluating the electrocatalytic activity of a CE.

$$J_0 = \frac{RT}{nFR_{ct}} \qquad (4)$$

where R is the gas constant; n (n=2) is the number of electrons involved in the reduction of triiodide at the electrode; D is the diffusion coefficient of the triiodide; l is the spacer thickness; T is the temperature; F is Faraday's constant; C is the triiodide concentration.

Thus, the order of R_{ct} will be inferred to NiS/PEDOT < Pt < PEDOT < NiS CEs from J_0, implying the most

excellent electrocatalytic activity for the NiS/PEDOT CE in I^-/I_3^- redox couple, which can be logically expected considerably improved the efficiency of DSSC. The conclusions are consistent with the catalytic activity derived from the EIS and CV.

3.3 Photovoltaic performance of DSSCs with NiS/PEDOT CE

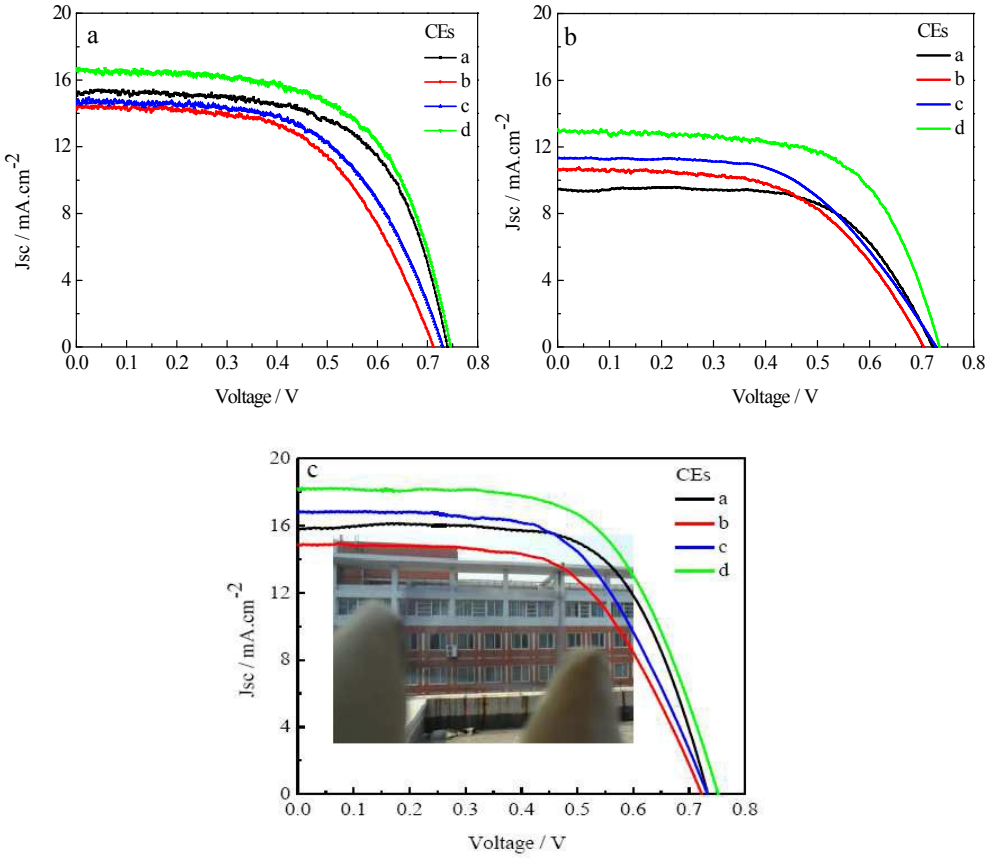

Fig. 8 Photocurrent density-voltage curves of the DSSCs.

Fig. 8 shows the photovoltaic properties of DSSCs based on different CEs and directions under the illumination of 100 mW·cm^{-2} and the detailed photovoltaic parameters are summarized in Table 2. Fig. 8a shows *J-V* curves of the DSSCs with the Pt (a), NiS (b), PEDOT (c) and NiS/PEDOT (d) CEs irradiated only from the front and without aluminum foil as the reflector, from which obtained the *PCEs* are of 7.14%, 6.18%, 5.80% and 7.77%, respectively. The DSSC based on the NiS/PEDOT (d) CE achieved as high as *PCE* of 7.77%, higher than that of the DSSC with Pt, PEDOT or NiS CE only. The greatly improved in performance of the DSSC assembled with NiS/PEDOT CE possibly be derived from the synergistic catalytic effect of NiS and PEDOT for their excellent intrinsic electrocatalytic activity and electrical conductivity, highly uniformity morphology provided the excellent

contact area for the CE and electrolyte. When irradiated from rear side, the *PCEs* of the DSSCs with the Pt and NiS CEs reduced more than that of the DSSCs based on the PEDOT and NiS/PEDOT CEs as shown in Fig. 8b. This is due to the decrease in incident light intensity via the reflection of Pt and NiS CEs, thus diminishes the photogenerated charge carriers and light-to-electric conversion efficiency.

Interestingly, it can be obtained from Fig. 8c that the DSSCs assembled with Pt CE irradiated from front and using a piece of new aluminum foil as the reflector achieves the *PCE* of 7.30%, higher than that of the DSSCs with NiS and PEDOT CEs. Low efficiency for the DSSCs with NiS and PEDOT CEs is responsible for their CE low electrocatalytic activity and high resistances derived from Fig. 4 and Fig. 6, and the low transmittance of NiS CE. Compared with the DSSC with NiS CE, the efficiency and short-circuit current density of the DSSC with PEDOT CE irradiated from the rear are remarkably reduced less, the mainly reason is the higher transmittance of PEDOT CE than that of NiS CE. The DSSC with NiS/PEDOT CE obtained *PCE* is as high as 8.47% with aluminum foil as the reflector, which increases 9.0% than that of the DSSC from front irradiation only. Due to the transparency and excellent electrocatalytic ablity of NiS/PEDOT CE, rear light penetrated and be absorbed by the dye molecules and produced more photogenerated charge carriers in device, resulting greatly enhanced the short-circuit current density and power conversion efficiency. This strategy can be further improved by designing a better light-splitting device with vertical incidence and applied other devices with transparent CEs.

Table 2 The photovoltaic performance parameters of DSSCs with various counter electrodes.

CEs and irradiarion direction	V_{oc} (V)	J_{sc} (mA·cm^{-2})	*FF*	*PCE* (%)
Pt, front front & rear	0.733	15.81	0.63	7.30
Pt, front	0.739	15.33	0.63	7.14
Pt, rear	0.723	9.46	0.62	4.24
NiS, front & rear	0.719	14.87	0.60	6.41
NiS, front	0.712	14.54	0.56	5.80
NiS, rear	0.704	10.67	0.55	4.13
PEDOT, front & rear	0.730	16.81	0.59	7.24
PEDOT, front	0.730	14.85	0.57	6.18
PEDOT, rear	0.728	11.34	0.55	4.54
NiS/PEDOT, front & rear	0.751	18.19	0.62	8.47
NiS/PEDOT, front	0.746	16.79	0.62	7.77
NiS/PEDOT, rear	0.734	12.96	0.62	5.89

3.4 Schematic of the catalytic mechanisms of samples

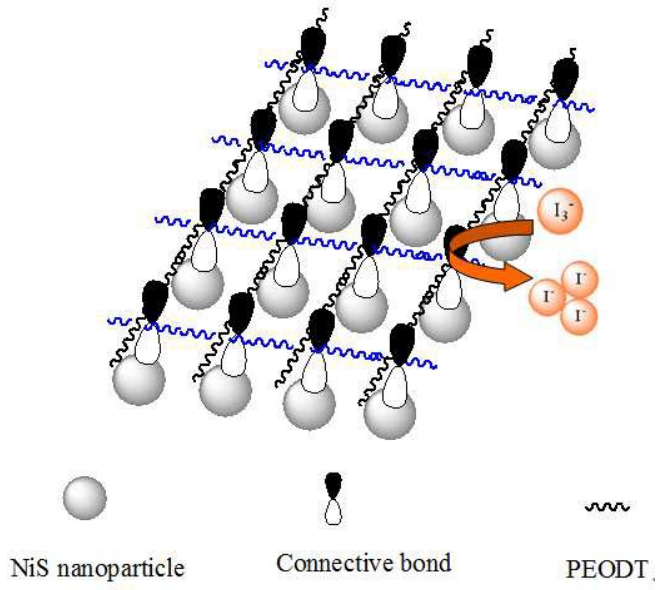

Fig. 9 Schematic of the catalytic mechanisms of NiS/PEDOT CE.

Fig. 9 shows the possible catalytic mechanisms of NiS/PEDOT CE in I_3^- electrolyte during the power conversion efficiency process for the DSSC. Firstly, 4-ATP was introduced as a bridging agent via a covalent bonding between NiS and -SH end on 4-ATP and an in-situ growth of PEDOT chain on $-SH_2$ end on 4-ATP, showing a much better electrochemical behavior to iodide/triiodide. Furthermore, owing to the incorporation of highly conductive PEDOT network into the NiS nanoparticles introduces more pathways for electron transport and therefore facilitates the charge transfer across the CE/electrolyte interface, directly resulting in a higher electrocatalytic activity of the NiS/PEDOT CE and the consequent enhancement in the photovoltaic performance.

4. Conclusions

A transparent NiS/PEDOT counter electrode with significantly enhanced electrochemical performance was prepared by two-step electrochemical/chemical process, and proposed as Pt-free counter electrode catalyst for DSSCs. As evidenced SEM images, NiS nanoparticles and PEDOT net-work integrated tightly, intercross and penetrate, provide efficient pathways for electron transport and favors the permeation of iodide/triiodide electrolyte and the sunlight transmission. Electrochemical studies indicate that the synergistic effect of the NiS and PEDOT can efficiently facilitate the electron transport and therefore enhance the charge-transfer rate for I_3^- reduction. Consequently, the DSSC assembled with the NiS/PEDOT counter electrode achieves an impressive

PCE of 8.47% under the irradiation from the front and aluminum foil as the reflector, which is greatly enhanced the power conversion efficiency than that of the DSSC irradiated from front only (7.77%). The strategy of enhanced efficiency for DSSC is with the advantages of low-cost, easy fabrication, high throughput and therefore provides a new route for enhancing the photovoltaic performance of solar cells and other photovoltaic systems with transparent CEs.

Acknowledgements

The authors are very grateful to the joint support by the National Natural Science Foundation of China (No. 21103041). This work is also supported by the Natural Science Foundation of Henan Educational Committee (No. 14A430023) and the Scientific Research Found of Henan Provincial Department of Science and Technology (No. 132300413210).

References

[1] B. O'Regan, M. Grätzel, *Nature*, 1991, **353**, 737–740.

[2] M. Grätzel, *Nature*, 2001, **414**, 338–344.

[3] S. Mathew, A. Yella, P. Gao, R. Humphry-Baker, B. F. E. Curchod, N. Ashari-Astani, I. Tavernelli, U. Rothlisberger, M. K. Nazeeruddin, M. Grätzel, *Nat. Chem*., 2014, **6**, 242–247.

[4] A. Kay, M. Grätzel, *Sol. Energy Mater. Sol. Cells*, 1996, **44**, 99–117.

[5] T. Chen, L. Qiu, Z. Yang, Z. Cai, J. Ren, H. Li, H. Lin, X. Sun, H. Peng, *Angew. Chem., Int. Ed*., 2012, **51**, 11977–11980.

[6] L. Kavan, J. Yum, M. Grätzel, *Nano Lett*., 2011, **11**, 5501–5506.

[7] G.T. Yue, J.H. Wu, Y.M. Xiao, J.M. Lin, M.L. Huang, Z. Lan, *J. Phys. Chem. C*, 2012, **116**, 18057–18063.

[8] Q.H. Li, J.H. Wu, Q.W. Tang, Z. Lan, P.J. Li, J.M. Lin, *Electrochem. Commun*., 2008, **10**, 1299–1302.

[9] J. Jang, D. Ham, E. Ramasamy, J. Lee, J.S. Lee, *Chem. Commun*., 2010, **46**, 8600–8602.

[10] G. Li, J. Song, G. Pan, X. Gao, *Energy Environ. Sci*., 2011, **4**, 1680–1683.

[11] M. Wu, J. Bai, Y. Wang, A. Wang, X. Lin, L. Wang, Y. Shen, Z. Wang, A. Hagfeldt, T. Ma, *J. Mater. Chem.*, 2012, **22**, 11121–11127.

[12] Y. Hou, D. Wang, X. H. Yang, W. Q. Fang, B. Zhang, H. F. Wang, G. Z. Lu, P. Hu, H. J. Zhao, H. G. Yang, *Nat. Commun.*, 2013, **4**, 1583.

[13] Z.L. Ku, X. Li, G.H. Liu, H. Wang, Y.G. Rong, M. Xu, L.F. Liu, M. Hu, Y. Yang, H.W. Han, *J. Mater. Chem. A*, 2013, **1**, 237–240.

[14] L.J. Sun, Y. Bai, K.N. Sun, *RSC Adv.*, 2014, **4**, 42087–42091.

[15] G.T. Yue, J.H. Wu, Y.M. Xiao, M.L. Huang, J.M. Lin, J.Y. Lin, *J. Mater. Chem. A*, 2013, **1**, 1495–1501.

[16] Z.L. Hu, K. Xia, J. Zhang, Z.Y. Hu, Y.J. Zhu, *RSC Adv.*, 2014, **4**, 42917–42923.

[17] G.T. Yue, X.P. Ma, Q.W. Jiang, F.R. Tan, J.H. Wu, C. Chen, F.M. Li, Q.H. Li, *Electrochim. Acta*, 2014, **142**, 68–75.

[18] H.C. Sun, D. Qin, S.Q. Huang, X.Z. Guo, D.M. Li, Y.H. Luo, Q.B. Meng, *Energy Environ. Sci.*, 2011, **4**, 2630–2637.

[19] Y.M. Xiao, J.-Y. Lin, S.-Y. Tai, S.u-W. Chou, G.T. Yue, J.H. Wu, *J. Mater. Chem*., 2012, **22**, 19919–19925.

[20] F. Gong, H. Wang, X. Xu, G. Zhou, Z. Wang, *J. Am. Chem. Soc*., 2012, **134**, 10953–10958.

[21] S. Ito, S.M. Zakeeruddin, P. Comte, P. Liska, D. Kuang, M. Grätzel, *Nat. Photonics*, 2008, **2**, 693–698.

[22] Q. Tai, B. Chen, F. Guo, S. Xu, H. Hu, B. Sebo, X.Z. Zhao, *ACS Nano*, 2011, **5**, 3795–3799.

[23] G. T. Yue, F.M. Li, F.R. Tan, G.Q. Li, C. Chen, J.H. Wu, *RSC Adv*., 2014, **4**, 64068–64074.

[24] L. Jiao, Z. Wang, L. Niu, J. Shen, T.Y. You, S.J. Dong, A. Ivaska, *J. Solid State Electrochem.*, 2006, **10**, 886–893.

[25] J.H. Wu, Y.M. Xiao, G.T. Yue, Q.W. Tang, J.M. Lin, M.L. Huang, Y.F. Huang, L.Q. Fan, Z. Lan, S. Yin, T. Sato, *Adv. Mater.*, 2012, **24**, 1884–1888

[26] G.T. Yue, X.A. Zhang, L. Wang, F.R. Tan, J.H. Wu, Q.W. Jiang, J.M. Lin, M.L. Huang, Z. Lan, *Electrochim. Acta*, 2014, **129**, 229–236.

[27] M.Y. Yen, C.K. Hsieh, C.C. Teng, M.C. Hsiao, P.I. Liu, C.C.M. Ma, M.C. Tsai, C.H. Tsai, Y.R. Lin, T.Y. Chou, *RSC Adv.*, 2012, **2**, 2725–2728.

[28] G.T. Yue, W.F. Zhang, J.H. Wu, Q.W. Jiang, *Electrochim. Acta*, 2013, **112**, 655–662.

[29] J.Y. Lin, J.H. Liao, T.Y. Hung, *Electrochem. Commun.*, 2011, **13**, 977–980.

[30] J.H. Wu, G.T. Yue, Y.M. Xiao, S.Y. Tai, M.L. Huang, J.M. Lin, L.Q. Fan, Z. Lan, J.Y. Lin, *ACS Appl. Mater. Interfaces*, 2012, **4**, 6530–6536.

[31] A. Hauch, A. Georg, *Electrochim. Acta*, 2001, **46**, 3457–3466.

[32] M.-H. Yeh, L.-Y. Lin, C.-P. Lee, H.-Y. Wei, C.-Y. Chen, C.-G. Wu, R. Vittal, K.-C. Ho, *J. Mater. Chem.*, 2011, **21**, 19021–12029.

[33] S.M. Zakeeruddin, M. Grätzel, *Adv. Funct. Mater.*, 2009, **19**, 2187–2202.

[34] G. Mor, K. Shankar, M. Paulose, O. Varghese, C. Grimes, *Nano Lett.*, 2006, **6**, 215–218.

[35] G.T. Yue, J.H. Wu, J.Y. Lin, Y.M. Xiao, J.M. Lin, M.L. Huang, Z. Lan, *Carbon*, 2013, **55**, 1−9.

[36] Q.W. Jiang, G.R. Li, X.P. Gao, *Chem. Commun.*, 2009, **44**, 6720−6722.

[37] M. Wang, A. M. Anghel, B. Marsan, N.-L. Cever Ha, N. Pootrakulchote, S. M. Zakeeruddin, M. Grätzel, *J. Am. Chem. Soc.*, 2009, **131**, 15976−15977.